Progress In Electromagnetics Research, PIER 80, 225–239, 2008

COMBINING MULTILEVEL GREEN'S FUNCTION INTERPOLATION METHOD WITH VOLUME LOOP BASES FOR INDUCTANCE EXTRACTION PROBLEMS

H. G. Wang and P. Zhao

The Electromagnetics Academy at Zhejiang University
Zhejiang University
Hangzhou 310058, China

Abstract—In this paper, a fast integral equation method is developed for extracting the inductances in RF ICs, RF MEMs, IC packages, and deep submicron ICs etc. This method combines a recently developed Multilevel Green's Function Interpolation Method (MLGFIM) [1, 2] with the volume integral equation discretized using Volume Loop (VL) basis functions. In it, instead of using the filaments model to simulate the currents flowing in the inductors, we use the conventional SWG basis functions for this kind of basis functions is flexible for problems with complex geometries. The shortest path finding algorithm is also used to find the source loop basis functions. The inductance extractions from the straight line, the spiral inductors, the bump, and the parallel buses in this paper demonstrate the validity and efficiency of this hybrid method.

1. INTRODUCTION

Inductance extractions are important issues in designing RFICs, RF MEMs, IC packages, and deep submicron ICs. We can view this kind of problems as the low frequency electromagnetic problems [3]. A lot of methods [4–6] can be used to solve this kind of problems. The structures we studied are conductors such as interconnects used in deep submicron techniques [7], spiral inductors used in RFIC [8] and RF MEMs [9], and bumps used in IC packages [10]. The sizes of them are in micron and deep submicron scales, while using Method of Moments (MoM), we can no longer simply consider them as the Perfect Electric Conducting problems as in [11]. In [12], the filaments model is used to model the currents. The advantage of filaments model is that it is simple and efficient for modeling the straight line segments. However,

if the structures become complex, e.g., the sphere bumps in which the currents with more than one directions flow unevenly, filaments model can hardly be used in meshing them. SWG basis functions [13] are one of the well known basis functions used to model volume displacement currents. For quasistatic problems, because of the EM decoupling, recently developed loop tree bases or loop-star bases [14–18] based on SWG bases should be employed to make the MoM matrix equation stable. Moreover, for the magneto-quasistatic problems, only volume loop bases are needed for modeling the divergence free currents [15, 18]. After obtaining a MoM matrix equation using the volume loop basis in discretizing the volume integral equation, one needs to find a fast equation solver.

There exist a lot of fast integral equation methods that can be used to enhance the efficiency of the solution, for instance, FMM [12, 19–21], CGFFT [22, 23], Pre-corrected FFT [24], SMCG [25], AIM [26], IceCube [27], IMLMQRF [11, 28], and MLGFIM [1, 2] and so on. In them, 1) FMM is the fastest method with $O(N)$ complexity for quasistatic problems; 2) SMCG, CGFFT, Pre-corrected FFT, SMCG, and AIM are FFT based methods with $O(N \log N)$ complexity; 3) Ice Cube and IMLMQRF are the methods based on matrix compression technique, i.e., QR factorization, matrix merging, and matrix column and row sampling techniques; 4) MLGFIM is based on a hierarchical structure that is similar to FMM but using the Green's function matrix interpolation method with QR factorization technique. This method has a complexity of $O(N)$ [1]. It has been developed for solving full-wave problems by adopting radial basis functions.

In this paper, we will use MLGFIM with radial basis function interpolation technique to extract the parasitic inductances that are encountered in RFICs, RFMEMs and IC packages. We first use the volume integral equation with volume loop bases to describe this kind of problems. Consequently, instead of obtaining the volume loop impedance matrix, we use the method similar to the mesh analysis introduced in [12]. However, we adopt the SWG bases instead of the filaments modeling, because SWG bases are more flexible for modeling the volume objects with complex shapes. For the source voltage excitation and the source loop basis functions, we find the source path using the shortest path algorithm [29]. Then, the MLGFIM-Volume Loop Algorithm that is suitable for magneto-quasistatic problems is developed. The numerical results in this paper show the validity and efficiency of MLGFIM-VL.

2. COMBINATION OF MLGFIM WITH VOLUME LOOP BASES IN LOW FREQUENCY

For inductance extraction problems, the mixed potential integral equation can be written as.

$$\boldsymbol{E} - \frac{i\omega\mu_0}{4\pi}\int\limits_{\Omega} dv' \frac{\exp(ik|\boldsymbol{r}-\boldsymbol{r}'|)}{|\boldsymbol{r}-\boldsymbol{r}'|}\cdot \boldsymbol{J}_{eq}(\boldsymbol{r}') = -\nabla\phi, \tag{1}$$

where

$$\begin{aligned}\boldsymbol{J}_{eq}(\boldsymbol{r}) &= [-i\omega(\varepsilon(\boldsymbol{r})-\varepsilon_0)]\boldsymbol{E}(\boldsymbol{r})\\ &= \tau(\boldsymbol{r})\boldsymbol{E}(\boldsymbol{r})\\ &= \frac{-i\omega(\varepsilon(\boldsymbol{r})-\varepsilon_0)}{-i\omega\cdot\varepsilon(\boldsymbol{r})}\cdot(-i\omega)\cdot\varepsilon(\boldsymbol{r})\boldsymbol{E}(\boldsymbol{r})\\ &= (1-\varepsilon_0/\varepsilon(\boldsymbol{r}))\cdot[-i\omega\cdot\varepsilon(\boldsymbol{r})\boldsymbol{E}(\boldsymbol{r})]\\ &= \kappa(\boldsymbol{r})\cdot[-i\omega\boldsymbol{D}(\boldsymbol{r})].\end{aligned} \tag{2}$$

Here, $\varepsilon(\boldsymbol{r}) = \varepsilon_0(\boldsymbol{r}) + i\frac{\sigma}{\omega}$, ε_0 is the dielectric constant of the free space, σ is the conductivity. Employing the volume loop bases set $\{\boldsymbol{o}_i\}_{i=1}^{N_L}$, expanding the displacement current as $-i\omega\boldsymbol{D} = \sum\limits_{i=1}^{N_L} I_i\cdot\boldsymbol{o}_i$, and applying the Galerkin method, (1) can be converted to

$$\bar{\bar{Z}}'\cdot\bar{I} = \bar{V}, \tag{3}$$

where

$$\begin{aligned}Z'_{mn} &= -i\omega\mu_0\int\limits_{\Omega_m} dv\int\limits_{\Omega_n} dv'\boldsymbol{o}_m(\boldsymbol{r})\cdot\bar{\boldsymbol{G}}_A\cdot\kappa(\boldsymbol{r}')\boldsymbol{o}_n(\boldsymbol{r}')\\ &\quad+\int\limits_{\Omega_m} dv\boldsymbol{o}_m(\boldsymbol{r})\cdot\kappa(\boldsymbol{r})\boldsymbol{o}_n(\boldsymbol{r})/\tau(\boldsymbol{r}),\end{aligned} \tag{4}$$

and Ω_i is the support of the i-th volume loop basis function.

$$V_m = -\int\limits_{\Omega_m} dv\boldsymbol{o}_m(\boldsymbol{r})\cdot\nabla\phi. \tag{5}$$

Here we define the loop bases as the combination of the SWG bases, viz.,

$$\boldsymbol{o}_m(\boldsymbol{r}) = \sum_{i=1}^{N} P_{m,i}\cdot\boldsymbol{j}_i, \tag{6}$$

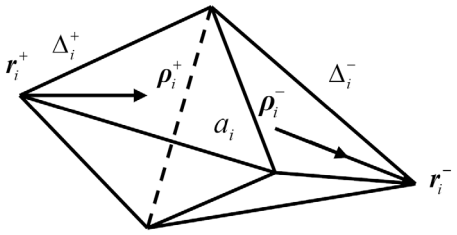

Figure 1. The support of a SWG basis function. It consists of two adjacent tetrahedrons.

where $\{\boldsymbol{j}_i\}_{i=1}^N$ is the SWG bases set, and N is the number of SWG bases used to model the problem. It is known that the SWG bases can be written as [13]

$$\boldsymbol{j}_i(\boldsymbol{r}) = \begin{cases} \dfrac{\boldsymbol{\rho}_i^+}{3\Delta_i^+}, & \boldsymbol{r} \in T_i^+ \\ \dfrac{\boldsymbol{\rho}_i^-}{3\Delta_i^-}, & \boldsymbol{r} \in T_i^- \end{cases}, \tag{7}$$

where $T_i^{\pm}$ are the two adjacent tetrahedrons supporting $\boldsymbol{j}_i$ and and $\Delta_i^{\pm}$ are the corresponding volumes of these two tetrahedrons, while $\boldsymbol{\rho}_i^+ = \boldsymbol{r} - \boldsymbol{r}_i^+$ or $\boldsymbol{\rho}_i^- = \boldsymbol{r} - \boldsymbol{r}_i^-$ and $\boldsymbol{r}_i^{\pm}$ denote the two vertices as shown in Fig. 1. Consequently, (4) can be rewritten as

$$\begin{aligned} Z'_{mn} &= \sum_{i=1}^{N}\sum_{j=1}^{N} P_{m,i}P_{n,j}\Bigg\{ -i\omega\mu_0 \int\limits_{\diamondsuit_i} dv \int\limits_{\diamondsuit_j} dv' \boldsymbol{j}_i(\boldsymbol{r}) \cdot \bar{\boldsymbol{G}}_A \cdot \kappa(\boldsymbol{r}')\boldsymbol{j}_j(\boldsymbol{r}') \\ &\quad + \int\limits_{\diamondsuit_j} dv \boldsymbol{j}_i(\boldsymbol{r}) \cdot \kappa(\boldsymbol{r})\boldsymbol{j}_j(\boldsymbol{r})/\tau(\boldsymbol{r}) \Bigg\} \\ &= \sum_{i=1}^{N}\sum_{j=1}^{N} P_{m,i}P_{n,j}Z_{i,j}, \end{aligned} \tag{8}$$

where $\diamondsuit_i$ is the support of the i-th SWG basis function. Thus, Equation (3) can be rewritten as

$$\bar{\bar{P}} \cdot \bar{\bar{Z}} \cdot \bar{\bar{P}}^T \cdot \bar{I} = \bar{V}, \tag{9}$$

where $\bar{\bar{P}}$ is a $N_L - by - N$ sparse matrix that can be easily generated according to the relation (6). One of the advantages of applying (9)

rather than (3) is that no rewriting of the impedance matrix calculation program is needed when one already has the Method of Moments program developed using SWG bases.

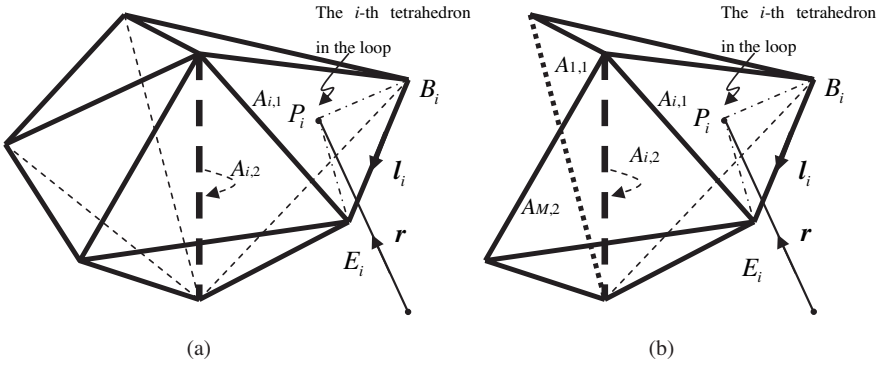

Figure 2. The support of a loop basis function.

The loop bases are classified into the closed loop bases and the unclosed loop bases whose supports are shown in Figs. 2(a) and (b), respectively. In tetrahedron i of a loop basis function support, the loop basis function (in which the subscript m is omitted for simplicity) can be expressed as $\boldsymbol{o}(\boldsymbol{r}) = \frac{\boldsymbol{l}_i}{3\Delta_i}$. We will prove that (5) becomes zero if the support of the loop basis function is closed and otherwise it equals the voltage between the two ends of the unclosed loop. This is shown in Equation (10).

$$\begin{aligned} V &= -\sum_{i=1}^{M} \int_{T_i} dv\, \boldsymbol{o}(\boldsymbol{r}) \cdot \nabla\phi = -\sum_{i=1}^{M} \int_{T_i} dv \nabla \cdot \boldsymbol{o}(\boldsymbol{r})\phi = -\sum_{i=1}^{M} \oint_{T_i} d\boldsymbol{S} \cdot \boldsymbol{o}(\boldsymbol{r})\phi \\ &= -\sum_{i=2}^{M} \left[\int_{A_{i,2}} d\boldsymbol{S} \cdot \boldsymbol{l}_i(\boldsymbol{r})\phi/3\Delta_i + \int_{A_{i,1}} d\boldsymbol{S} \cdot \boldsymbol{l}_i(\boldsymbol{r})\phi/3\Delta_i \right] \\ &= -\left\{ \sum_{i=1}^{M-1} \left[\int_{A_{i,2}} d\boldsymbol{S} \cdot \boldsymbol{l}_i(\boldsymbol{r})\phi/3\Delta_i + \int_{A_{i+1,1}} d\boldsymbol{S} \cdot \boldsymbol{l}_{i+1}(\boldsymbol{r})\phi/3\Delta_{i+1} \right] \right. \\ &\quad \left. \int_{A_{1,1}} d\boldsymbol{S} \cdot \boldsymbol{l}_1(\boldsymbol{r})\phi/3\Delta_1 + \int_{A_{M,1}} d\boldsymbol{S} \cdot \boldsymbol{l}_M(\boldsymbol{r})\phi/3\Delta_M \right\} \end{aligned}$$

$$
\begin{aligned}
&= -\left\{ \sum_{i=2}^{M-1} \left[\frac{h_{i,2}}{3\Delta_i} - \frac{h_{i+1,1}}{3\Delta_{i+1}} \right] \int_{A_{i,2}} \phi dS - \frac{h_{1,1}}{3\Delta_1} \int_{A_{1,1}} \phi dS + \frac{h_{M,2}}{3\Delta_M} \int_{A_{M,2}} \phi dS \right\} \\
&= -\left\{ \sum_{i=2}^{M-1} \left[\frac{h_{i,2}}{3\Delta_i} - \frac{h_{i+1,1}}{3\Delta_{i+1}} \right] A_{i,2}\ \phi(\boldsymbol{\xi})|_{\boldsymbol{\xi} \in A_{i,2}} \right. \\
&\quad \left. - \frac{h_{1,1}}{3\Delta_1} A_{1,1} \phi(\boldsymbol{\xi})\ |_{\boldsymbol{\xi} \in A_{1,1}} + \frac{h_{M,2}}{3\Delta_2} A_{M,2} \phi(\boldsymbol{\xi})\ |_{\boldsymbol{\xi} \in A_{M,2}} \right\} \\
&= -\{0 - \phi(\boldsymbol{\xi})|_{\boldsymbol{\xi} \in A_{1,1}} + \phi(\boldsymbol{\xi})|_{\boldsymbol{\xi} \in A_{M,2}}\} \\
&= \begin{cases} 0, & \text{if the loop is closed.} \\ \phi(\boldsymbol{\xi})|_{\boldsymbol{\xi} \in A_{M,2}} - \phi(\boldsymbol{\xi})|_{\boldsymbol{\xi} \in A_{1,1}}, & \text{other else.} \end{cases}
\end{aligned} \tag{10}
$$

where M is the number of tetrahedrons of the loop basis function and $h_{i,1}$ and $h_{i,2}$ are the height respectively perpendicular to areas $A_{i,1}$ and $A_{i,2}$ that are shown in Fig. 2. In (10) we have used the integration middle-value theorem.

For a conductor of finite conductivity meshed with tetrahedrons, if we can find a path of interconnected tetrahedrons between the two ends of this conductor, we can generate an unclosed source loop basis function called $\boldsymbol{o}_n$ whose support is the path, and impose the voltage between its two ends. Because the topological structure of the meshed geometry is stored as a graph, we can use the shortest path finding method to find this path [29]. Fig. 3 shows an inductor structure and its corresponding shortest path using the shortest path finding algorithm. This path builds the support of the unclosed loop basis function. After it, we impose one volt voltage between the two ends of the conductor, and thus the corresponding excitation entry $V_n = 1$, viz., $\bar{V} = [0 \cdots, 1, \cdots 0]^T$.

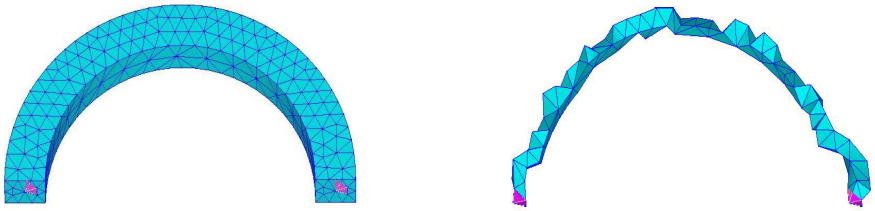

(a) (b)

Figure 3. (a) An inductor structure. (b) The shortest path between its two ends.

Now, we have fully described the method of generating Equation (9). In the following, we employ MLGFIM to accelerate the matrix-vector multiplication $\bar{\bar{Z}} \cdot \bar{x}$ (where $\bar{x} = \bar{\bar{P}}^T \cdot \bar{I}$,) in (9).

First, the impedance matrix entries $Z_{i,j}$ are decomposed into

$$Z_{i,j} = Z_{i,j}^x + Z_{i,j}^y + Z_{i,j}^z, \tag{11}$$

where

$$Z_{i,j}^* = \int\limits_{\diamondsuit_i} dv \int\limits_{\diamondsuit_j} dv' j_i^*(\boldsymbol{r}) j_j^*(\boldsymbol{r}') \kappa(\boldsymbol{r}') G_0(\boldsymbol{r}, \boldsymbol{r}'). \tag{12}$$

Similarly as in [2], Equations (12) can be written as a generic form.

$$\hbar_{i,j} = \int\limits_{\diamondsuit_i} dv \int\limits_{\diamondsuit_j} dv' \tau_i(\boldsymbol{r}) \tau_j(\boldsymbol{r}') \kappa(\boldsymbol{r}') G_0(\boldsymbol{r}, \boldsymbol{r}'). \tag{13}$$

Assume that the supports of basis function i and j are respectively in two well separated cubes G_m and G_n. The Green's function can be approximated using radial basis function interpolation technique as shown in [1, 2]:

$$\begin{aligned} G_0(\boldsymbol{r}, \boldsymbol{r}') &= \sum_{p=1}^{K} \sum_{q=1}^{K} \omega_{m,p}(\boldsymbol{r}) \omega_{n,q}(\boldsymbol{r}') G_0(\boldsymbol{r}_{G_m,p}, \boldsymbol{r}_{\boldsymbol{G_n},q}) \\ &= \bar{\omega}_m^T(\boldsymbol{r}) \cdot \bar{\bar{G}}_{mn} \cdot \bar{\omega}_n(\boldsymbol{r}'), \end{aligned} \tag{14}$$

where $\omega_{m,p}(\boldsymbol{r})$ and $\omega_{n,q}(\boldsymbol{r}')$ (defined in Appendix A of [1]) are the p-th radial basis interpolation polynomials in cube G_m and q-th radial basis interpolation polynomials in cube G_n, respectively; $G_0(\boldsymbol{r}_{\boldsymbol{G_m},p}, \boldsymbol{r}_{\boldsymbol{G_n},q})$ is the Green's function value generated from interpolation point $\boldsymbol{r}_{G_n,q}$ in cube G_n to interpolation point $\boldsymbol{r}_{G_m,p}$ in cube G_m; K is the number of interpolation points in G_m or G_n. Here, we choose the $3^3 + 2^3$ Tartan grid presented in [2]. Substituting (14) into (13) gives

$$\begin{aligned} \hbar_{i,j} &= \int\limits_{\diamondsuit_i} dv \int\limits_{\diamondsuit_j} dv' [\tau_i(\boldsymbol{r}) \tau_j(\boldsymbol{r}')] \bar{\omega}_m^T(\boldsymbol{r}) \bar{\bar{G}}_{m,n} \bar{\omega}_n(\boldsymbol{r}') \kappa(\boldsymbol{r}') \\ &= \left[\int\limits_{\diamondsuit_i} dv \tau_i(\boldsymbol{r}) \bar{\omega}_m^T(\boldsymbol{r}) \right] \bar{\bar{G}}_{m,n} \left[\int\limits_{\diamondsuit_j} dv' \tau_j(\boldsymbol{r}') \bar{\omega}_n(\boldsymbol{r}') \kappa(\boldsymbol{r}') \right] \\ &= \bar{v}_{m,i}^T \cdot \bar{\bar{G}}_{m,n} \cdot \bar{v}'_{n,j}. \end{aligned} \tag{15}$$

In (15), $\bar{v}'_{n,j}$ is not equal to $\bar{v}_{n,i}$. For the case that $\kappa(\boldsymbol{r}')$ is constant over the problem region, $\bar{v}'_{n,j} = \kappa \cdot \bar{v}_{n,j}$. For finite conductor case, $\kappa(\boldsymbol{r}') \simeq 1$, hence $\bar{v}'_{n,j} \simeq \bar{v}_{n,j}$. For the case that $\kappa(\boldsymbol{r}')$ is variant, we adopt the approximation $\bar{v}'_{n,j} \simeq \kappa_j \cdot \bar{v}_{n,j}$, where κ_j is the average $\kappa(\boldsymbol{r}')$ in the support of the j-th SWG basis function. Thus (15) can be rewritten as

$$\hbar_{i,j} = \bar{v}^T_{m,i} \cdot \bar{\bar{G}}_{m,n} \cdot \bar{v}_{n,j} \cdot \kappa_j. \tag{16}$$

Consequently, following the similar steps in [2], the Algorithm for calculating $\bar{b} = \bar{\bar{Z}} \cdot \bar{x}$, i.e., MLGFIM-Volume Loop is listed below.

Algorithm 1. MLGFIM-VL.

Step 0 *Modify the value of* $\bar{x}$ *by* $Diag[\kappa_1, \cdots, \kappa_i, \cdots, \kappa_N] \cdot \bar{x}$. *The complexity is* $O(N)$.

Step 1 *Call algorithm 1 in* [2], *but without calculating the term for scalar potential, because in the problem of this paper, no scalar potential is needed for building the MoM matrix. Note that here the radial basis function interpolation with 35 Tartan grid interpolation points is applied at all levels. The threshold for QR compressing the Green's function matrix is chosen to be* 10^{-2}.

The differences between MLGFIM-VL and the algorithm in [2] are 1) the elements in $\bar{v}_{n,i}$ of (16) is obtained by volume integration instead of surface integration; 2) step 0 is added to consider the variant dielectric contrast factor $\kappa(\boldsymbol{r})$; 3) the number of interpolation points is $K_l = K = 35$ at all levels so that the algorithm has a complexity of $O(N)$; that has been proved in [1]. Moreover, the QR factorization technique used in [2] has also been used here for compressing the Green's function matrices $\bar{\bar{G}}_{m_l,l;n_l,l}$ at level l, where $l = 2, \cdots, L$.

3. NUMERICAL RESULTS

In this section, we calculate all the examples using GMRES iterative solver. The inner loop of GMRES contains 200 matrix-vector multiplications. The threshold is set to be 1×10^{-4}. The matrix-vector multiplication calculation is accelerated using MLGFIM-VL.

The first example is a rectangular straight Cu line ($\sigma = 5.961 \times 10^7$ S/m) with 5 microns by 30 microns by 1000 microns as shown in Fig. 4(a). The calculated inductances of this straight line at 2 GHz and 10 GHz are listed in Table 1. We use the solutions by Fast Henry solver as the reference solution, because Fast Henry can give a fast and

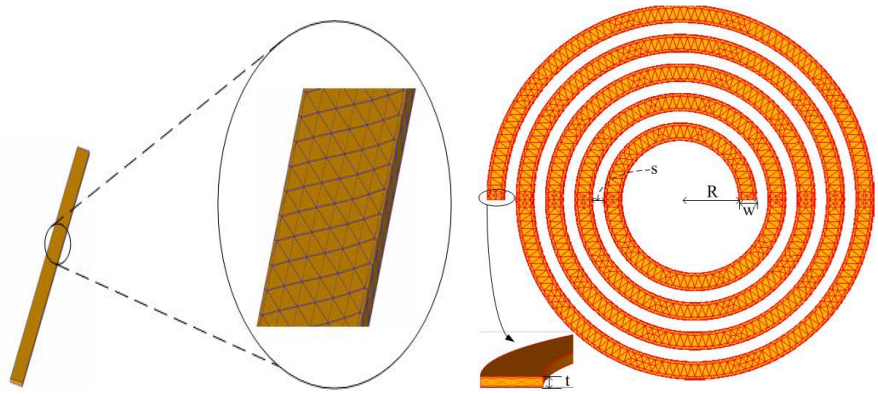

(a) (b)

Figure 4. (a) A rectangular straight line with 5 microns by 30 microns by 1000 microns. (b) A 4.5 turns inductor. $w = 30$ microns, $t = 3$ microns, $s = 20$ microns, and $R = 100$ microns.

accurate result for quasi static problems with regular shapes such as straight lines.

The second example is for the Cu spiral inductors ($\sigma = 5.961 \times 10^7$ S/m) that are often used in RF ICs or RF MEMs. The geometry shape and size of this kind of inductors is shown in Fig. 4(b). The width w, thickness t, space s, and inner radius R are 30, 3, 20, and 100 microns respectively. Table 1 lists the inductances calculated by MLGFIM-VL for inductors with different turns. The results obtained by FastHenry software are also listed for comparisons. While applying FastHenry, we dissect the inductor into a lot of very small curved blocks and model these curved blocks using rectangular blocks that are called by FastHenry solver. We see that our results agree well with that of FastHenry software with differences restricted in 5%.

The third example as shown in Fig. 5(a) is for the bumps used in IC packages. Because of the curve feature of the spherical bump, it is not convenient to use Fasthenry in modeling this structure. However, the tetrahedron elements used in our method are very flexible for geometry with complex shape. We investigate a Au bump ($\sigma = 4.521 \times 10^7$ S/m) at 10 GHz with the sizes R_1, R_2, R_3, H_1, H_2, and H_3 being 50, 30, 20, 40, 10, 10 microns, respectively. Fig. 5(b) shows the inductance results calculated by our method with different number of meshed SWG bases. We see that the result converges when the mesh density increases. The difference between the value obtained using the smallest number of SWG bases (10,563) and that obtained using the biggest number of

Table 1. Inductances of the straight line and spiral inductors.

Examples	Frequency	Inductance (nH)		
		MLGFIM-VL	Fast Henry	Difference (%)
Straight line (in Fig. 3)	2 GHz	0.884541	0.884935	0.04
	10 GHz	0.881354	0.898938	1.95608
1.5 turns spiral inductor	13 Hz	0.981343	0.994345	1.30759
	13 GHz	0.942563	0.966121	2.43841
2.5 turns spiral inductor	6.3 Hz	2.56795	2.60564	1.44648
	6.3 GHz	2.46407	2.54221	3.07370
3.5 turns spiral inductor	4.4 Hz	5.08489	5.21537	2.50184
	4.4 GHz	4.89556	5.10688	4.13795
4.5 turns spiral inductor	2.8 Hz	8.81897	9.02001	2.22882
	2.8 GHz	8.50109	8.85870	4.03682

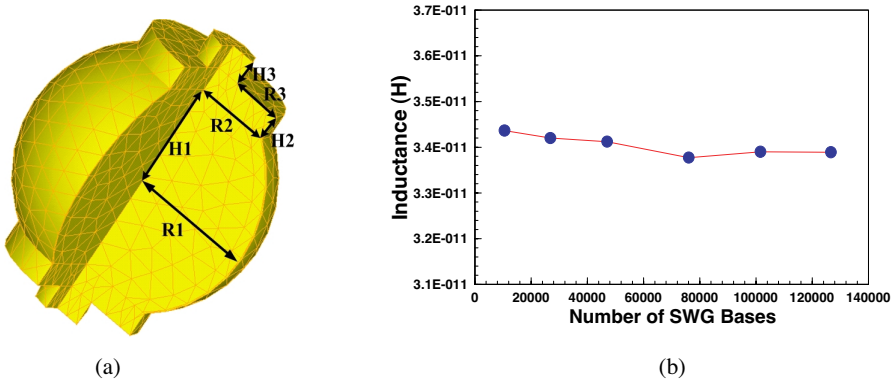

(a) (b)

Figure 5. (a) The inner view of a volume meshed Au bump. (b) The inductance of this bump.

SWG bases (126,653) is only 1.4%. This confirms the validity and accuracy of MLGFIM-VL.

The fourth example is the mutual inductances extractions among the parallel interconnect buses in deep submicron ICs. The mutual inductances will cause noise and delay effects on other neighbor lines [7]. So, correctly predicting their values is very important for the designers to work out remedy. Fig. 6(a) illustrates three parallel Cu ($\sigma = 5.961 \times 10^7$ S/m) buses. The sizes W, T, and L are 0.13, 0.4, and 34.97 microns respectively. Fig. 6(b) shows the mutual inductances among them versus the space between them.

Table 2. Mutual inductances of the three parallel lines calculated by MLGFIM-VL and fasthenry (UNIT: 10^{-11}H).

S (microns)	Calculated by MLGFIM-VL			Calculated by FastHenry solver			Difference (%)
	Self inductance	Between two neighbor buses	Between two apart buses	Self inductance	Between two neighbor buses	Between two apart buses	
0.13	3.67954	3.12654	2.71350	3.81043	3.15633	2.74687	2.48040
0.39	3.67955	2.71347	2.25841	3.81043	2.74687	2.26466	2.60635
0.65	3.67955	2.44842	1.98861	3.81043	2.46294	1.98943	2.69154
0.91	3.67953	2.25841	1.79901	3.81044	2.26467	1.79739	2.77793
1.17	3.67952	2.10960	1.65357	3.81044	2.11621	1.65572	2.84900
1.43	3.67955	1.98866	1.53651	3.81044	1.98943	1.53393	2.90621

Table 2 lists the mutual inductance values calculated by our method and FastHenry solver. We see that the differences are confined in 3%. The difference is calculated by formula $\left\|\bar{\bar{L}}_{MLGFIM-VL} - \bar{\bar{L}}_{FASTHENRY}\right\|_F / \left\|\bar{\bar{L}}_{FASTHENRY}\right\|_F$, where the subscript F denotes the Frobenius Norm.

MLGFIM-VL.

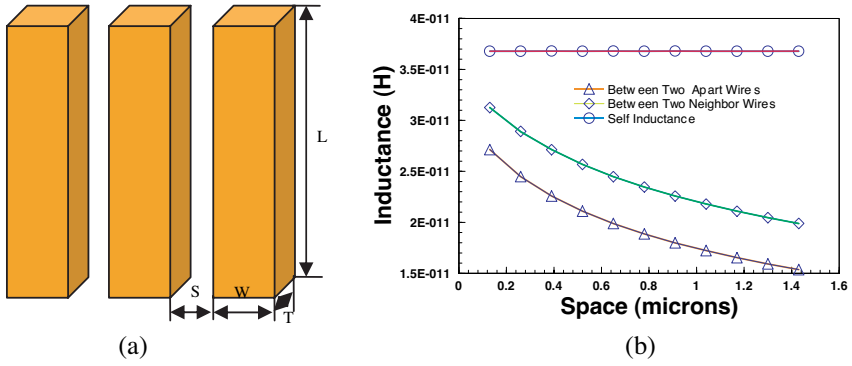

(a) (b)

Figure 6. (a) Three parallel interconnect buses in deep sub-micron ICs. (b) Self and mutual inductances among the three parallel buses.

In Fig. 7, we plot the memory requirement and the CPU time per matrix-vector multiplication in (9) for the spirals with 0.5, 1.5, 2.5, 3.5, and 4.4 turns and the Au bump with different number of SWG basis functions. The predicted values for MoM method is also

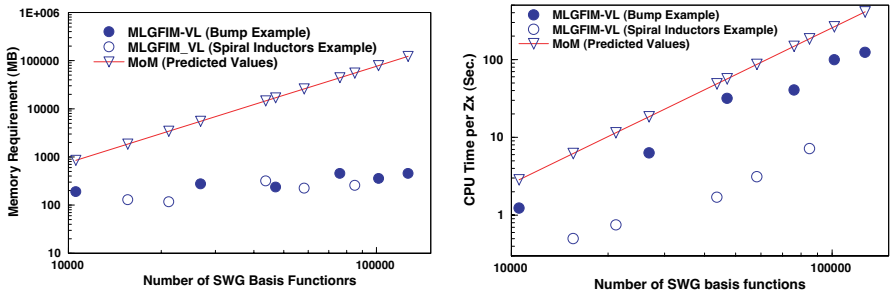

Figure 7. (a) The memory requirement versus the number of SWG bases. (b) The CPU time used per matrix-vector multiplication versus number of SWG bases.

draw for comparisons. Here $1\,\mathrm{MB} = 1024^2$ Bytes. We calculate a 0.5 turn spiral inductor with 1153 SWG bases using MoM and record the used CPU time in per matrix-vector multiplication. According to the square law of the complexity of MoM, we can predict the CPU time used per matrix-vector multiplication versus any number of SWG basis functions. From Fig. 7(a), we see that using MLGFIM-VL can significantly save the memory. From Fig. 7(b), we also see that the time saving for bump example is less significant than that for the inductors example. The main reason is that because the number of cubes in the *interaction list* [1] of a 3D solid structure is always $6^3 - 3^3 = 189$, while that for a 2D structure is $6^2 - 3^2 = 27$, so the time used in the *interaction phase* [2] for 3D solid cases, e.g., the bump, should be about 7 times of that for 2D structures, e.g., the spiral inductors. Nevertheless, in Fig. 7(b), we observe that for both cases, the time used in MLGFIM-VL per matrix-vector multiplication should be significantly less than that used in MoM. Following the increase of the number of SWG basis functions, this significance will be more and more drastic.

4. CONCLUSION

In this paper, we develop a fast integral equation method for extracting the inductances in RF ICs, RF MEMs, IC packages, and deep submicron ICs etc. This method combines Multilevel Green's Function Interpolation Method (MLGFIM) with the volume integral equation discretized using Volume Loop (VL) basis functions. In it, instead of using the filaments model, we use the conventional SWG basis functions for this kind of basis functions is flexible for problems with

complex geometries. We also use the shortest path finding algorithm to find the source loop basis functions. The inductance extractions from the straight line, the spiral inductors, the bump, and the parallel buses in this paper demonstrate the validity and efficiency of MLGFIM-VL.

ACKNOWLEDGMENT

This work was supported by Provincial Nature Science Foundation of Zhejiang, China No. Y105477, and National Nature Science Foundation of China No. 60501017.

REFERENCES

1. Wang, H. G., C. H. Chan, and L. Tsang, "A new multilevel Green's function interpolation method for large scale low frequency EM simulations," *IEEE Trans. Comput.-Aided Des. Integr. Circuits Syst.*, Vol. 24, No. 9, 1427–1443, Sep. 2005.
2. Wang, H. G. and C. H. Chan, "The implementation of multilevel Green's function interpolation method for full-wave electromagnetic problems," *IEEE Trans. Antennas Propag.*, Vol. 55, No. 5, 1348–1358, May 2007.
3. Venkov, G., M. W. McCall, and D. Censor, "The theory of low-frequency wave physics revisited," *Journal of Electromagnetic Waves and Applications*, Vol. 21, No. 2, 229–249, 2007.
4. Tang, W., X. He, T. Pan, and Y. L. Chow, "Synthetic asymptote formulas of equivalent circuit components of square spiral inductors," *Journal of Electromagnetic Waves and Applications*, Vol. 20, No. 2, 215–226, 2006.
5. Zheng, Q. and H. Zeng, "Multipole theory analysis of 3D magnetostatic fields," *Journal of Electromagnetic Waves and Applications*, Vol. 20, No. 3, 389–397, 2006.
6. Babic, S. I. and C. Akyel, "New mutual inductance calculation of the magnetically coupled coils: Thin disk coil-thin wall solenoid," *Journal of Electromagnetic Waves and Applications*, Vol. 20, No. 10, 1281–1290, 2006.
7. Hodges, D. A., H. G. Jackson, and R. A. Saleh, *Analysis and Design of Digital Integrated Circuits in Deep Submicron Technology*, McGraw-Hill Education (Asia) Co. and Tsinghua University Press, 2003.
8. Ulrich, R. K. and L. W. Schaper, *Integrated Passive Component Technology*, IEEE Press, Piscataway, NJ, 2003.

9. Varadan, V. K., K. J. Vinoy, and K. A. Jose, *RF MEMS and Their Applications*, John Wiley & Sons Inc., Hoboken, NJ, 2003.
10. Kusamitsu, H., Y. Morishita, K. Maruhashi, M. Ito, and K. Ohata, "The flip-chip bump interconnection for millimeter-wave GaAs MMIC," *IEEE Trans. Electronics Packaging Manufacturing*, Vol. 22, No. 1, 23–28, Jan. 1999.
11. Wang, H. G., C. H. Chan, L. Tsang, and V. Jandhyala, "On sampling algorithms in multilevel QR factorization method for magnetoquasitatic analysis of integrated circuits over multilayered lossy substrates," *IEEE Trans. Comput.-Aided Des. Integr. Circuits Syst.*, Vol. 25, No. 9, 1777–1792, Sep. 2006.
12. Kamon, M., M. J. Tsuk, and J. K. White, "FASTHENRY: A multipole accelerated 3-D inductance extraction program," *IEEE Trans. Microw. Theory Tech.*, Vol. 42, No. 9, 1750–1758, Sep. 1994.
13. Schaubert, D. H., D. R. Wilton, and A. W. Glisson, "A tetrahedral modeling method for electromagnetic scattering by arbitrarily shaped inhomogeneous dielectric bodies," *IEEE Trans. Antennas Propag.*, Vol. 32, No. 1, 77–85, Jan. 1984.
14. Rubin, B. J., "Divergence-free basis for representing polarization current in finite-size dielectric regions," *IEEE Trans. Antennas Propagat.*, Vol. 41, No. 3, 269–277, Mar. 1993.
15. Zhao, J. S. and W. C. Chew, "Integral equation solution of Maxwell's equations from zero frequency to microwave frequencies," *IEEE Trans. Antennas Propagat.*, Vol. 48, No. 10, 1635–1645, Oct. 2000.
16. Chen, S., W. C. Chew, J. M. Song, and J. S. Zhao, "Analysis of low frequency scattering from penetrable scatterers," *IEEE Trans. on Geoscience and Remote Sensing*, Vol. 39, No. 4, 726–735, April 2001.
17. Lee, J. F., R. Lee, and R. J. Burkholder, "Loop star basis functions and a robust pre-conditioner for EFIE scattering problems," *IEEE Trans. Antennas Propagat.*, Vol. 51, No. 8, 1855–1863, Aug. 2003.
18. Li, M.-K. and W. C. Chew, "Applying divergence-free condition in solving the volume integral equation," *Progress In Electromagnetics Research*, PIER 57, 311–333, 2006.
19. Rokhlin, V., "Rapid solution of integral equation of classical potential theory," *J. Comput. Phys.*, Vol. 60, 187–207, 1985.
20. Lu, C. C. and W. C. Chew, "A multilevel algorithm for solving boundary integral equations of wave scattering," *Microw. Opt. Tech. Lett.*, Vol. 7, 466–470, Jul. 1994.

21. Song, J. M., C. C. Lu, and W. C. Chew, and S. W. Lee, "Fast illinois solver code (FISC)," *IEEE Antennas Propag. Mag.*, Vol. 48, 27–34, Jun. 1998.
22. Sarkar, T. K., E. Arvas, and S. M. Rao, "Application of FFT and the conjugate gradient method for the solution of electromagnetic radiation from electrically large and small conducting bodies," *IEEE Trans. Antennas Propagat.*, Vol. 34, 635–640, May 1986.
23. Zhao, L., T. J. Cui, and W.-D. Li, "An efficient algorithm for EM scattering by electrically large dielectric objects using Mr-Qeb iterative scheme and CG-FFT method," *Progress In Electromagnetics Research*, PIER 67, 341–355, 2007.
24. Phillips, J. R. and J. K. White, "A precorrected-FFT method for electrostatic analysis of complicated 3-D structures," *IEEE Trans. Comput.-Aided Des. Integr. Circuits Syst.*, Vol. 16, 1059–1072, Oct. 1997.
25. Chan, C. H., C.-M. Lin, L. Tsang, and Y. F. Leung, "A sparse matrix/canonical grid method for analyzing microstrip structures," *IEICE Trans. Electron.*, Vol. E80-C, No. 11, 1354–1359, Nov. 1997.
26. Bleszynski, E., M. Bleszynski, and T. Jaroszewicz, "AIM: Adaptive integral method for solving large-scale electromagnetic scattering and radiation problems," *Radio Sci.*, Vol. 31, 1225–1251, Sept.–Oct. 1996.
27. Kapur, S. and D. E. Long, "IES^3: Efficient electrostatic and electromagnetic simulation," *IEEE Computational Science and Engineering*, Vol. 5, 60–67, Oct.–Dec. 1998.
28. Wang, H. G., C. H. Chan, L. Tsang, and K. F. Chan, "Mixture effective permittivity simulations using IMLMQRF method on preconditioned EFIE," *Progress In Electromagnetics Research*, PIER 57, 285–310, 2006.
29. Gilberg, R. F. and B. A. Forouzan, *Data Structures: A Pseudocode Approach with C++*, Thomson Asia Pte Ltd and PPTPH, 2002.